SANDIA REPORT
SAND2011-9011
Unlimited Release
Printed November 2011

Ota City: Characterizing Output Variability from 553 Homes with Residential PV Systems on a Distribution Feeder

Matthew Lave, Joshua S. Stein, Abraham Ellis, Clifford W. Hansen, Eichi Nakashima, and Yusuke Miyamoto

Prepared by
Sandia National Laboratories
Albuquerque, New Mexico 87185 and Livermore, California 94550

Sandia National Laboratories is a multi-program laboratory managed and operated by Sandia Corporation, a wholly owned subsidiary of Lockheed Martin Corporation, for the U.S. Department of Energy's National Nuclear Security Administration under contract DE-AC04-94AL85000.

Issued by Sandia National Laboratories, operated for the United States Department of Energy by Sandia Corporation.

Available to DOE and DOE contractors from
U.S. Department of Energy
Office of Scientific and Technical Information
P.O. Box 62
Oak Ridge, TN 37831

Telephone: (865) 576-8401
Facsimile: (865) 576-5728
E-Mail: reports@adonis.osti.gov
Online ordering: http://www.osti.gov/bridge

Available to the public from
U.S. Department of Commerce
National Technical Information Service
5285 Port Royal Rd.
Springfield, VA 22161

Telephone: (800) 553-6847
Facsimile: (703) 605-6900
E-Mail: orders@ntis.fedworld.gov
Online order: http://www.ntis.gov/help/ordermethods.asp?loc=7-4-0#online

SAND2011-9011
Unlimited Release
Printed November 2011

Ota City: Characterizing Output Variability from 553 Homes with Residential PV Systems on a Distribution Feeder

Matthew Lave, Joshua S. Stein,
Abraham Ellis, and Clifford W. Hansen
Sandia National Laboratories
P.O. Box 5800
Albuquerque, New Mexico 87185-1033

Eichi Nakashima and Yusuke Miyamoto
Kandenko
2-7-14, Jonan, Mito City
Ibaraki, Japan

Abstract

This report describes in-depth analysis of photovoltaic (PV) output variability in a high-penetration residential PV installation in the Pal Town neighborhood of Ota City, Japan. Pal Town is a unique test bed of high-penetration PV deployment. A total of 553 homes (approximately 80% of the neighborhood) have grid-connected PV totaling over 2 MW, and all are on a common distribution line. Power output at each house and irradiance at several locations were measured once per second in 2006 and 2007. Analysis of the Ota City data allowed for detailed characterization of distributed PV output variability and a better understanding of how variability scales spatially and temporally. For a highly variable test day, extreme power ramp rates (defined as the 99th percentile) were found to initially decrease with an increase in the number of houses at all timescales, but the reduction became negligible after a certain number of houses. Wavelet analysis resolved the variability reduction due to geographic diversity at various timescales, and the effect of geographic smoothing was found to be much more significant at shorter timescales.

CONTENTS

FIGURES

1. INTRODUCTION

The Pal Town neighborhood of Ota City, Japan, is a unique test bed of high-penetration, distributed solar energy. The Japanese government's New Energy and Industrial Technology Development Organization (NEDO) installed solar photovoltaic (PV) panels on 553 rooftops in Pal Town (approximately 80% of the neighborhood), in a project titled, "Demonstrative research on clustered PV systems." All PV systems were grid-interconnected to a single distribution line to examine their influence on the line and to determine proper technologies to resolve potential grid issues. Over 2 MW of distributed rooftop solar PV were installed in the roughly 0.4 km^2 neighborhood. Each rooftop PV system recorded its power output once per second in the years 2006 and 2007, and so this makes for an excellent location at which to study solar power variability.

1.1 Goals

1.1.1 Characterize Solar Power Variability at Various Timescales

The variability of solar power is an obstacle to high penetration, as it can lead to flicker, voltage fluctuations, and balancing problems. Variability is especially a problem at very short timescales (less than 1 hour), as expensive, fast-ramping spinning reserve must be used to counteract short-term fluctuations. Long-term fluctuations can be easier to predict, and can be countered by slower ramping and hence cheaper power sources, but the often large magnitude of long-term fluctuations means they can also add cost to PV integration. Due to the importance of both short and long timescales, we examine solar power variability in Pal Town at multiple timescales using ramp rate and wavelet-based analysis.

1.1.2 Determine How Solar Power Variability Scales With the Number of Houses

A key factor for solar power variability is geographic smoothing. While solar power at one site (i.e., one house) may be highly variable, the relative variability (variability relative to power capacity) will be reduced when many sites are added together (i.e., one neighborhood). This benefit will increase as more sites are added and as the correlation between sites is decreased. In this study, we determine the relationship between the relative variability and the number of sites for the Pal Town neighborhood.

1.2 Previous Works

1.2.1 Benefits of Geographic Smoothing

Many previous studies have shown reductions in variability of solar irradiance by adding multiple sites. Otani et al. (1997) use a fluctuation factor, defined as the root mean squared (RMS) value of a high-pass filtered 1-min time series of solar irradiance, to demonstrate a 2 to 5 times reduction in variability when considering nine sites located within a 4 km by 4 km grid. Curtright and Apt (2008) and Lave and Kleissl (2010) used 1-min timeseries to show reductions in the mean, maximum, and standard deviation of ramp rates (RRs) when considering the average of three or four sites (spread across Arizona and Colorado, respectively) versus only one

site. Power spectral densities (PSDs) presented in Otani et al. (1997), Curtright and Apt (2008), and Lave and Kleissl (2010) all show strong reductions in power content of fluctuations of the average of multiple sites versus the power content of fluctuations at one site.

Wiemken et al. (2001) examined 5-min normalized output from 100 PV sites spread throughout Germany, and found the standard deviation of the average of 100 sites to be reduced by a factor of 1.64 compared to 1 site for the month of June. They also discovered that 5-min fluctuations of ±5% of power output at nameplate capacity are virtually nonexistent in the average, yet single sites have fluctuations larger than ±50%.

1.2.2 Timescale Dependent Decorrelation

Murata et al. (2009) analyzed 1-min data from 52 PV systems spread across Japan to determine the "smoothing effect" of aggregating multiple systems. They found that over 1 min, sites more than about 50 to 100 km apart were uncorrelated, and thus there was a limit reached whereby adding more PV sites had no effect on reducing variability. For times greater than 10min, however, they reject the hypothesis that sites within 1000 km are independent, though some of the dependence may be due to diurnal solar cycles and could be eliminated by using a normalized solar radiation.

Mills and Wiser (2010) computed step changes (deltas) in clear-sky index for timeseries from the Southern Great Plains (SGP) Atmospheric Radiation Measurement (ARM) Program to test their model for solar irradiance variability as a function of distance across the plain. Fluctuations of 1 and 5 min showed nearly zero correlation between all 23 sites in the SGP network (sites range from 20 to 440 km apart), but deltas for times longer than 5 min increased in correlation with decreasing distance. The authors simulate a distributed PV plant consisting of 100 sites in a uniform 20 km by 20 km grid, and determine that six times less reserve resources are required to mitigate fluctuations for this distributed plant than would be required for a central plant of the same power capacity.

Perez et al. (2011) used 24 irradiance sensors – 17 stations in the ARM network and 7 stations in the SURFRAD network – to create virtual networks of irradiance sensors for studies of correlation. They find that 20-sec, 1-min, 5-min, and 15-min fluctuations become uncorrelated at 500 m, 1 km, 4 km, and 10 km, respectively. They extrapolate the found correlation relationships to model a homogeneously dispersed solar resource over a 40 by 40 km grid, and find variability to be reduced by a factor of 80, 40, 10, or 4 over the variability of a single site for timescales of 20 sec, 1 min, 5 min, or 15 min.

2. DATA

2.1 Description of Data

The Pal Town neighborhood of Ota City, Japan, contains 553 houses with rooftop PV systems (about 80% of the total houses in the neighborhood), ranging from 3 to 5 kW_p, making a total of 2.13 MW_p installed. The vast majority of houses (about 400 of the 553) had a 4 kW_p PV system. Most of the PV panels are either single or polycrystalline silicon. A map of Pal Town detailing the layout of houses with PV is shown in Figure 1. Since the PV panels are installed on domestic rooftops, the tilt and azimuth of the panels varies widely, as seen in Figure 2. The typical tilt of the PV panels is approximately 25° (more than half of the systems are between 23° to 27°), and the typical azimuth is south. The spacing between houses in Pal Town is large enough that shading from neighboring houses is not expected to be an issue.

In Pal Town, all household load and PV are connected to the same feeder, though there are also other loads on the feeder. The Pal Town feeder is a 6.6 kV overhead feeder, 3.26 km long from substation to Pal Town. The feeder connects to Pal Town near sensor 3 in Figure 1. Because all of the PV is on the same feeder, geographically concentrated, and the PV capacity is large relative to the household load, PV variability dominates net load variability of the Pal Town neighborhood (Figure 3). To help counter variability, batteries of 9 kWh were installed to all residences with PV systems in Pal Town. However, after several years of testing and analysis by NEDO, the batteries were withdrawn from operation as they were deemed unnecessary.

All houses collected PV power output data at 1-sec resolution. Additionally, there were six point sensors collecting GHI at 1-sec resolution using EKO instruments ML-020VM silicon pyranometers. The location of these point sensors is shown in Figure 1. Ota City receives slightly more sunlight annually than Tokyo, as the amount of solar insolation incident on a horizontal plane in Ota City is approximately 1.3 MWh m^{-2} yr^{-1}, 6% larger than in Tokyo.

Figure 1. Layout of the Pal Town neighborhood in Ota City. Black dots show houses with rooftop PV, and the red circles indicates the location of the GHI points sensors.

Figure 2. Photo of PV on the rooftops of houses in Pal Town.

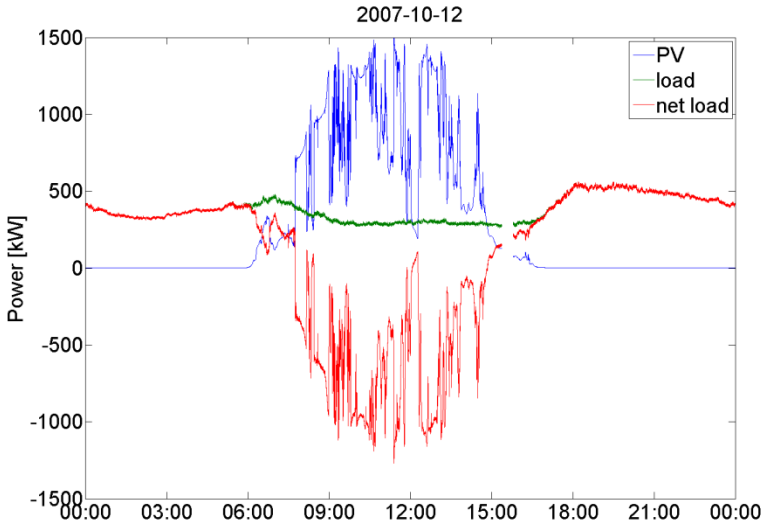

Figure 3. Aggregate PV generation, load, and net load (load-PV) for all of the Pal Town neighborhood on October 12, 2007. Since data was only available from 80% of the houses (those with PV), the load of those 80% was multiplied by 1.25 to estimate the load of all the houses in Pal Town connected to the same feeder, even those without rooftop PV. The unresolved period just after 15:00 is due to missing data.

2.2 Quality Control

2.2.1 No DC Power Data Available

The DC power output of the PV systems was chosen for this study due to the high level of apparent sensor noise on the AC data. However, a few of the Pal Town PV sites only had valid AC measurements, and so the number of houses available for this study was slightly reduced. The maximum number of sites reporting DC power data on one day was 483 (the number of sites with valid DC power in 2006 and 2007 data fluctuated due to new installations, sensor error, etc.). This is still a very large number of houses and a high proportion of all Pal Town houses, and so will still produce representative results of output variability and geographic smoothing.

2.2.2 Artificial Ramps

Even if a site is reporting DC power data, it may still have issues. The most common issue is extreme ramps that are not representative of cloud-caused events. Figure 4 shows a few such events. These extreme ramps occur because the 1-sec data collection system stops when a blackout or voltage dip trips the system, or when it is unable to communicate with the PV site. At some sites, there are observed to be quite a few of these outages for about 10-sec durations, though some outages can last up to about a minute. Immediately before and after outages, there were typically slow ramps down to and away from zero, meaning the outage had an effect on the data for longer than when a zero value was recorded. To remove the outages from the data, times when the power output was less than 0.7% of capacity and the 3 min before and after these times were filtered out.

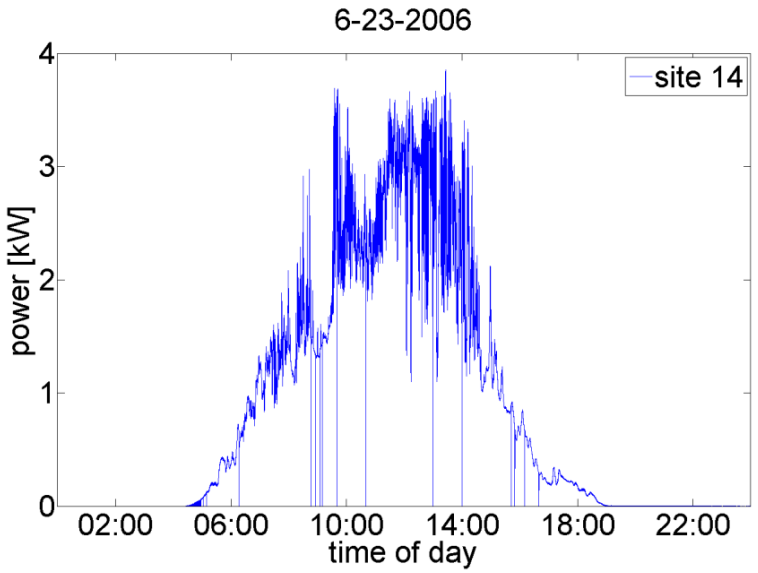

Figure 4. Power output from site 14 on June 23, 2006, shows extreme ramps down to zero power output, lasting about 10 seconds.

2.2.3 Correlation Filter

In addition to the data errors mentioned in Sections 2.2.1 and 2.2.2, there were some power output timeseries that deviated so far from the other timeseries that they were found to be errant. Figure 5 shows examples of these timeseries. To remove these largely deviating timeseries, a filter based on correlation between each timeseries and the mean of all timeseries was used. If the daytime (solar altitude angle > 10°) correlation between the two was less than 0.8 for a given site, then that site was deemed errant and removed from the analysis. The strategy was to err on the side of excluding more sites than necessary in order to ensure that all retained sites were indeed accurate. For example, the blue line in Figure 5 is likely real output of a house with panel azimuths far to the west, but was excluded using the correlation filter. It was decided to err on the side of exclusion because including just one errant site could cause large errors in ramp rate analysis. This correlation filter seemed effective for all days. Figures 5 and 6 show the rejected and retained power output profiles for October 12, 2007. Only four "good" sites were rejected on this day, leaving 477 sites in the analysis, meaning that even by using this aggressive filter, less than 1% of the data have been eliminated. Visually, all of the sites retained look to be appropriate power output profiles.

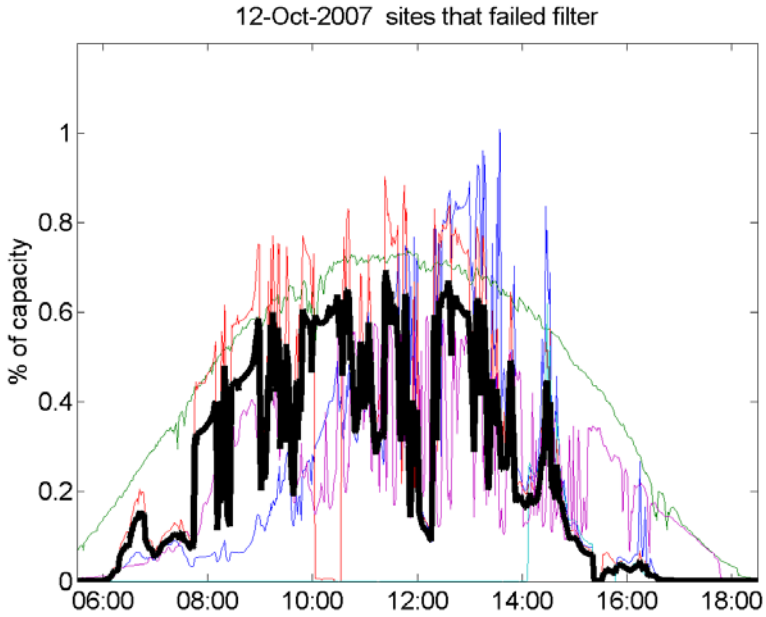

Figure 5. Power output as a percent of capacity (thin colored lines) for sites that failed the daytime correlation >0.8 filter. The mean of all sites is shown as the thick black line.

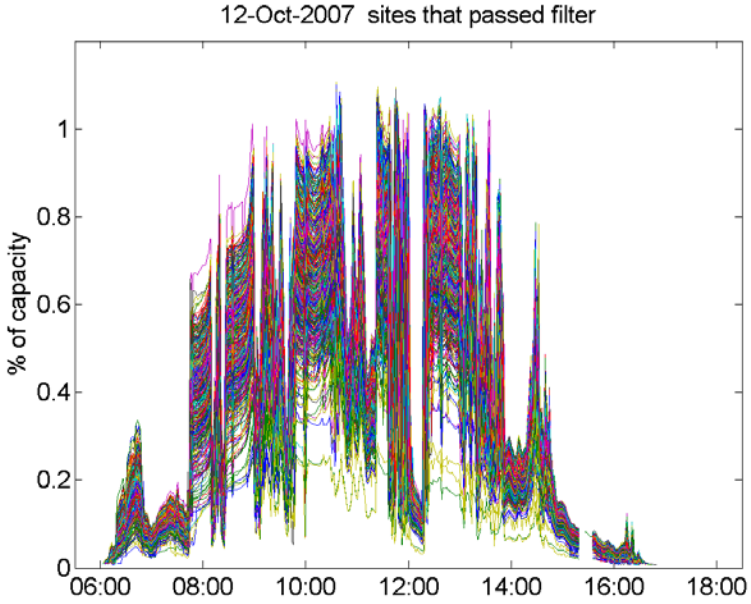

Figure 6. Power output as a percent of capacity for sites that passed the daytime correlation > 0.8 filter.

2.3 Test Day: October 12, 2007

October 12, 2007, was chosen as a test day for ramp rate statistics and wavelet analysis since it is a typical highly variable day with few errors in the data. This day is shown in Figure 3. A total of 477 houses passed the quality controls laid out in Sections 2.2.1 and 2.2.3 on October 12.

Additionally, when the measurements from a GHI point sensor were required, sensor 1 was used (see Figure 1 for sensor location). Sensor 1 was chosen because it is co-located with the project administrative office, so it is expected to be the best maintained and to produce the most reliable results.

3. METHODS

3.1 Ramp Rates

Extreme RRs of solar PV power are of critical interest to power system operators who need to understand worst-case scenarios. In this study the 99th-percentile RRs (RR99s) were calculated to gain an understanding of the worst-case fluctuations. RR99s were used instead of maximum RR for two reasons: (1) using RR99s, the worst-case scenarios that are seen somewhat often (1% of the time) and must be addressed are understood, while the maximum gives only the single worst-case scenario in a whole day, which may not be of consequence, and (2) using the RR99s is another method of quality controlling the data as it protects against the case where the maximum RR was an error in the data rather than an actual power change of the system.

After quality controlling the data as described in Section 2.2, the mean RR99 for the power output of a single house, and the RR99 of the aggregate power output of all houses, $P(t)$, were computed. $P(t)$ was obtained by summing all the individual houses, and so ignores transmission losses. To allow for easy comparison between individual houses and aggregate power output, RR99s were calculated as a function of system rated capacity. RR99s were calculated at 1 sec, 10 sec, 30 sec, 1 min, and 10 min. Timeseries corresponding to timescales longer than 1 sec were created by block-averaging the 1-sec timeseries, which simulates data collected once per timescale, and RR99s were computed based on the newly created timeseries. This method means that the length of the timeseries is shorter for longer timescales (i.e., there are 144 10-min block average values per day, versus 86,400 1-sec values).

Using longer time intervals than 10 min meant that too high of a percentage of the data had been thrown out due to quality control issues and so did not allow for accurate RR99s of the aggregate power output. RR statistics at longer timescales are well documented in other works (see, for example, Lave et al. 2011). While other studies have used the absolute value of RRs, in this report positive and negative ramps have been segregated, and so in addition to computing RR99s the 1st-percentile RRs (RR01s) were also calculated. Except for a negative sign, the RR99s and RR01s were found to be very nearly identical and so RR01s are not presented here. For comparison to other works, the RR99s in this study are equivalent to 98th-percentile absolute value RRs.

In order to obtain a better resolution of the behavior of RR99s as the number of houses increases, RR99s were computed for varying numbers of houses, N, from 2 to 400. The process to compute RR99s for *N* houses was as follows:

1. Select a random permutation of N houses. For example, for $N = 2$, the 25th and 400th houses might be chosen.
2. Find the average power output, as a function of capacity, for the combination of all N houses.
3. Determine the RR99 for this average power output.
4. Repeat steps 1 through 3 100 times to ensure that house selection is representative (if only done once, houses right next to each other might be picked, underrepresenting the geographic diversity of the neighborhood).
5. Record RR99 as the mean value of these 100 RR99 values computed in steps 1 through 4.

This method was run to find RR99s for timescales of 1 sec, 10 sec, 30 sec, 1 min, and 10 min for all days with data in 2007.

3.2 Wavelet Decomposition

To understand power fluctuations at each timescale, a wavelet transform can be used (see, for example, Woyte et al. 2007 or Lave et al. 2011). Since the wavelet transform works best upon a stationary signal, power output was first normalized by a clear-sky model such that output during entirely clear conditions would be 1. To create a clear-sky model for Pal Town, we used the Ineichen GHI clear-sky model to create GHI_{clr} (Ineichen and Perez 2002), and the Page Model to translate GHI into global irradiance on an inclined surface (Page 2003). An inclined surface 15° tilted from horizontal and positioned 10° east of south was found to best fit the data, and this is likely the average tilt and azimuth for all of Pal Town. To translate this irradiance model to a clear-sky power output model, the clear-sky global irradiance on the inclined surface was multiplied by the power capacity of Pal Town, and a constant conversion efficiency of 0.85, creating $P_{clr}(t)$. Temperature effects were found to be small (less than 5%), and varied from day to day, motivating the choice for a constant rather than temperature-dependent conversion efficiency. A normalized power output timeseries, essentially a power-derived clear-sky index, was created by dividing *P(t)* by $P_{clr}(t)$:

$$P_{norm}(t) = \frac{P(t)}{P_{clr}(t)}. \quad (1)$$

Since each house has panels at different orientations than its neighbors', it was not possible to fit a clear-sky curve to the individual houses. Instead, the GHI measurement, $GHI(t)$, was used from the 1st point sensor (as shown in Figure 1) as a proxy for a single house. The GHI was normalized to create a clear-sky index:

$$GHI_{norm}(t) = \frac{GHI(t)}{GHI_{clr}(t)}. \quad (2)$$

The wavelet transform of the power output timeseries, $P_{norm}(t)$, is:

$$w_j(t) = \int_{t_{min}}^{t_{max}} P_{norm}(T) \frac{1}{\sqrt{2^{j+1}}} \psi\left(\frac{T-t}{2^{j+1}}\right) dT, \quad (3)$$

where the wavelet timescale (length of fluctuations) in seconds is 2^j, and T is a variable of integration. The top hat wavelet was used, defined by:

$$\psi(t) = \begin{cases} 1, & \frac{1}{4} < t < 3/4 \\ -1, & 0 < t < \frac{1}{4} \quad || \quad \frac{3}{4} < t < 1 \\ 0, & else \end{cases}, \quad (4)$$

because of its simplicity and similarity to the shape of solar power fluctuations. Wavelet modes (timeseries) were computed for j values ranging from 1 (2 sec) to 12 (~1 hr), thus decomposing

the $P_{norm}(t)$ timeseries into 12 modes showing fluctuations at these various timescales. Symmetric signal extension was used to ensure resolution at endpoints. A special definition for the highest wavelet mode was adopted, defining $w_{12}(t)$ to be the moving average with window $2^{12} = 4096s$. By doing so, the property that the sum of all wavelet modes equals the original input signal is achieved:

$$\sum_{j=1}^{12} w_j(t) = P_{norm}(t). \tag{5}$$

The same wavelet transform was applied to the timeseries $GHI_{norm}(t)$, allowing for a comparison of fluctuations between the point sensor (representing a single house) and the areally average power output at each timescale. In addition to directly comparing the wavelet mode timeseries, the mathematical power content of each mode, called the fluctuation power index (fpi) can also be compared:

$$\text{fpi}(j) = \frac{1}{t_{min} - t_{max}} \int_{t_{min}}^{t_{max}} \frac{1}{2^{j+1}} \left| w_j(t) \right|^2 dt. \tag{6}$$

Comparing the fpi of GHI_{norm} to the fpi of P_{norm} gives an idea of the geographic smoothing effect. To quantify smoothing, the variability reduction (VR) is defined as:

$$\text{VR}(j) = \frac{\text{fpi}_{GHI_{norm}}(j)}{\text{fpi}_{P_{norm}}(j)}. \tag{7}$$

A high VR indicates strong geographic smoothing of the total power output versus the power output of a single house, while a VR of unity means no smoothing benefit.

4. RESULTS

4.1 99th-Percentile RRs

RR99s were found for various numbers of houses and timescales for the test day, and the results are shown in Figure 7. The RR99s are presented as change in percent of capacity per timescale of interest, meaning, for example, that a 1-min RR99 of 20% means a 20% change per minute. When normalized to RRs per second, the 1-sec RR99s are always larger than the longer-timescale RR99s. RR99s represent relative variability (% of capacity fluctuations), not absolute variability (fluctuations in kW). While relative variability is expected to decrease when adding more PV sites, absolute variability will increase since the total capacity of the system will also have increased.

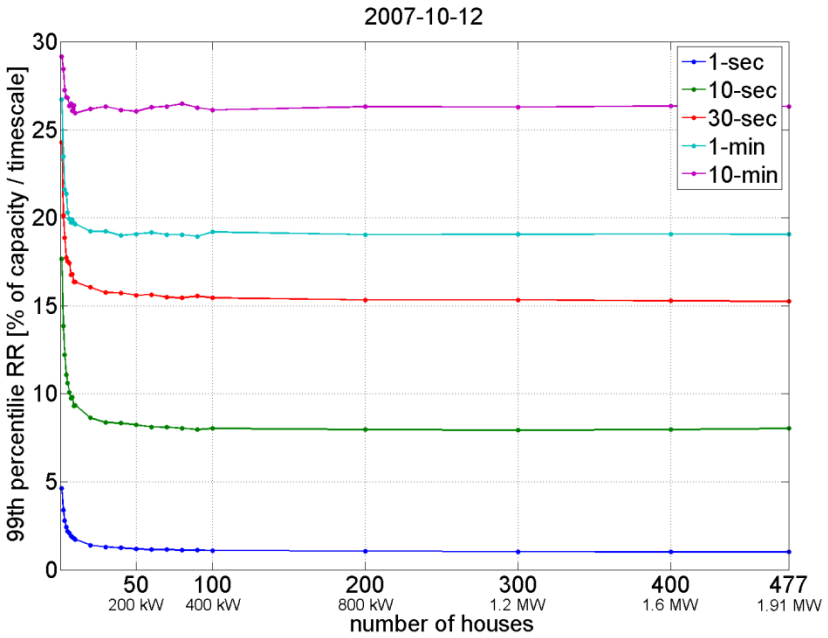

Figure 7. RR99s for various timescales and number of houses on October 12, 2007.

RR99s initially decrease significantly as more houses are added, but eventually reach a nearly steady value. To quantify the reduction in RR99 when adding more houses, Figure 8 shows the ratio of RR99 at one house to RR99 at many houses. When the ratio is large, there is a strong reduction in RR99, and when the ratio is 1, there is no reduction in RR99. The strongest reduction in RR99 is seen at 1 sec, where there is a more than 4.5 times reduction in RR99 of all 477 houses compared to RR99 of a single house. Additionally, at the 1-sec timescale, there continues to be a noticeable benefit to adding more sites. At longer timescales, there is almost no benefit to increasing from 100 to 477 sites. The 10-sec reduction in RR99 is still significant: more than a 2 times reduction in RR99 occurs for all 477 sites. At 10 min, however, the reduction in RR99 is minimal, indicating that 10-min RRs of a single house are similar to 10-min RRs of the entire 2-MW plant.

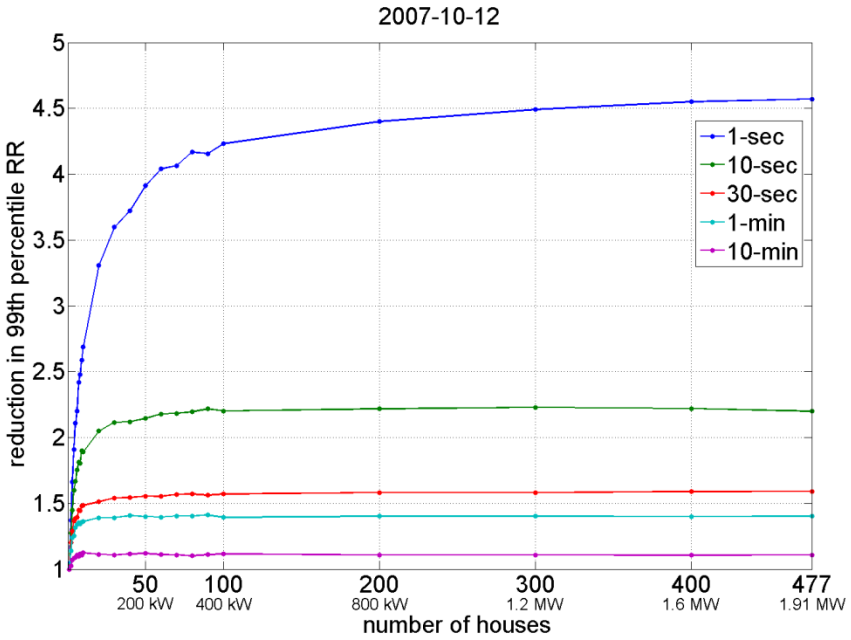

Figure 8. Ratio of RR99 of 1 house to RR99 of various numbers of houses on October 12, 2007. This plot can be used to determine the benefit of adding more houses. Large values indicate a strong reduction in RR99 compared to RR99 of a single house, while a value of 1 indicates no reduction in RR99.

Figures 7 and 8 show the RR99 behavior on the test day. To see how this compares to other days, Figure 9 shows the RR99s for various numbers of houses at timescales of 1 min and shorter for every day with data in 2007. On all days, RR99s decrease with increasing number of houses, though the rate of decrease varies from day to day. By comparing the test day (red line in Figure 9), to all other days, it is clear that the test day was one of the most variable days in the whole year. At every timescale, the test day has some of the highest RR99s.

Figure 9 also gives an indication of the most extreme RRs over the whole year. For example, at 1 sec there were only three RR99s greater than 1% of capacity in all of 2007, meaning for the sum of all PV in Pal Town it is very unlikely to have a RR99 greater than 1% of capacity. A much larger change can be expected over 1 min, where it is only unlikely to have RR99s over 20%. Note, though, that since the change happens over 1 minute, the rate of change is actually slower: a 1-min RR99 of 20% corresponds to a 1-sec RR99 of only 0.33%.

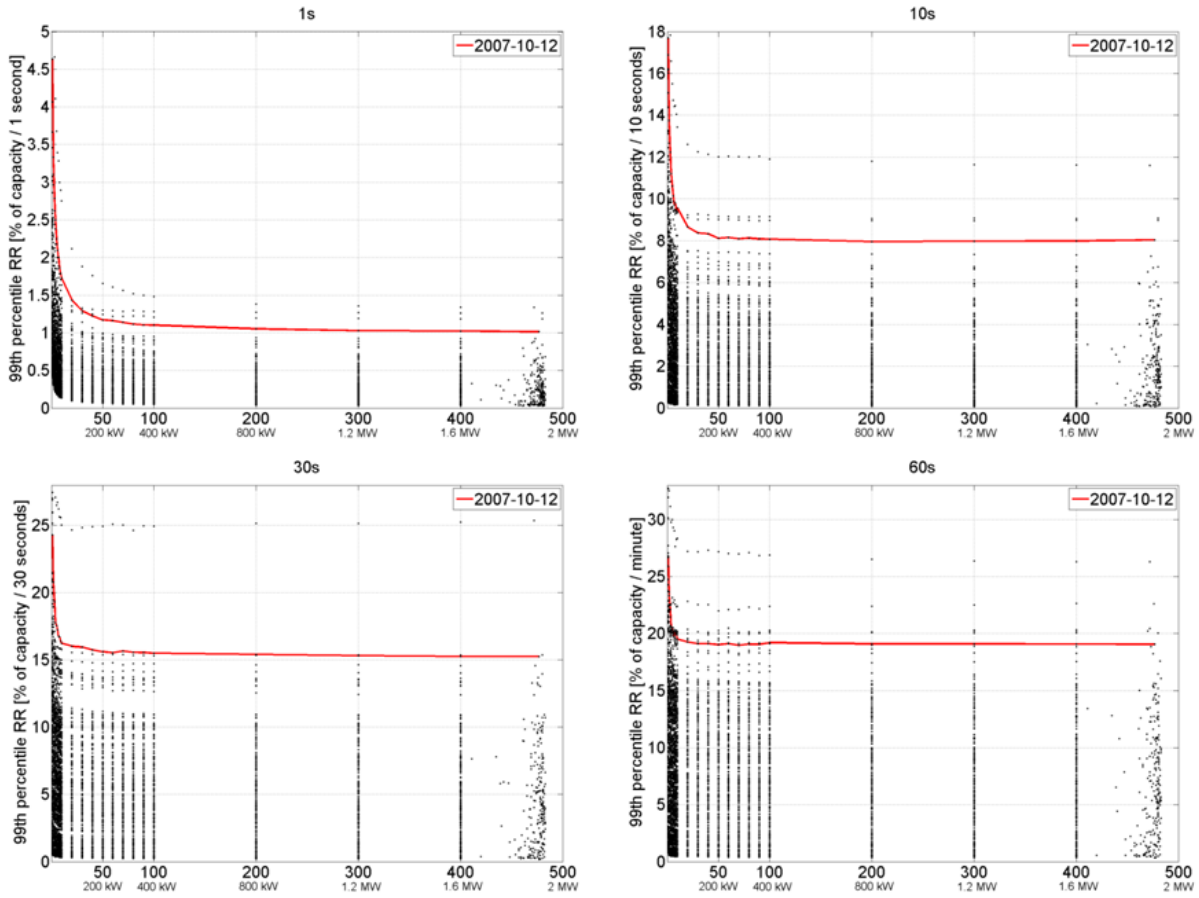

Figure 9. RR99s for every day with data in 2007 for 1-sec (top left), 10-sec (top right), 30-sec (bottom left), and 1-min (bottom right) timescales. The test day is shown as a red line, and is one of the days with the highest RR99s at all timescales. Note that the scale of the y-axis varies on each plot.

4.2 Wavelet Decomposition and Fluctuation Power Content

4.2.1 Wavelet Decomposition of a GHI Sensor and the Total Power Output of Pal Town

While RR statistics are often of interest to grid operators, RRs at a certain timescale are the combination of fluctuations at all timescales equal to and longer than the timescale under consideration. For example, in the morning, 1-min RRs will tend to be positive due to the longer-timescale effect of the sun rising. Using a wavelet decomposition allows fluctuations to be isolated by timescale. Wavelet decomposition using the top hat wavelet was calculated for $GHI_{norm}(t)$ and $P_{norm}(t)$, and both decompositions are shown in Figure 10.

The j=12 mode is not computed using Equation (3), but rather is a moving average with a window of 4096 sec. This preserves the identity that summing the wavelet modes $j = 1$ through $j = 12$ (2nd through 13th plots in Figure 10) will return the original input signal (top-most plot in Figure 10). This is important in that the GHI_{norm} or P_{norm} signals have not been altered, but merely separated by timescales. For example, a large weather front bringing a large cloud bank would be isolated to a long timescale, while a small hole in that cloud bank would be isolated to a short timescale. For RRs, the larger cloud back could overwhelm the small hole and lead to a negative short-timescale ramp, but with a wavelet decomposition the two events are separated.

At long timescales (large j values), the amplitude of fluctuations in P_{norm} is only slightly reduced over GHI_{norm}. This means that there is essentially no reduction in variability when averaging over all of Pal Town at long timescales, and is expected because clouds and weather fronts corresponding to long wavelet timescales will be large enough that they will cover all of Pal Town and affect the neighborhood uniformly. For example, if clouds were assumed to be moving overhead at a constant speed of 5 m/s with no distortion, a 1-km (the diagonal distance across Pal Town) cloud covering the whole neighborhood would correspond to a wavelet timescale of about 200 sec. Although assuming undistorted cloud motion is a crude approximation, it does appear that timescales greater than 200 sec have very similar wavelet modes of P_{norm} and GHI_{norm}.

At short timescales, however, there is a difference between P_{norm} and GHI_{norm} fluctuations. At $j = 1$ (2 sec) the difference is most extreme, as there are no noticeable fluctuations in P_{norm}, but are observable fluctuations in GHI_{norm}. For all shorter timescales ($j < 8$), there is a reduction in the magnitude of fluctuations of P_{norm} versus GHI_{norm}. At short timescales, therefore, there is a strong benefit to geographic smoothing, and this benefit decreases with increasing timescale.

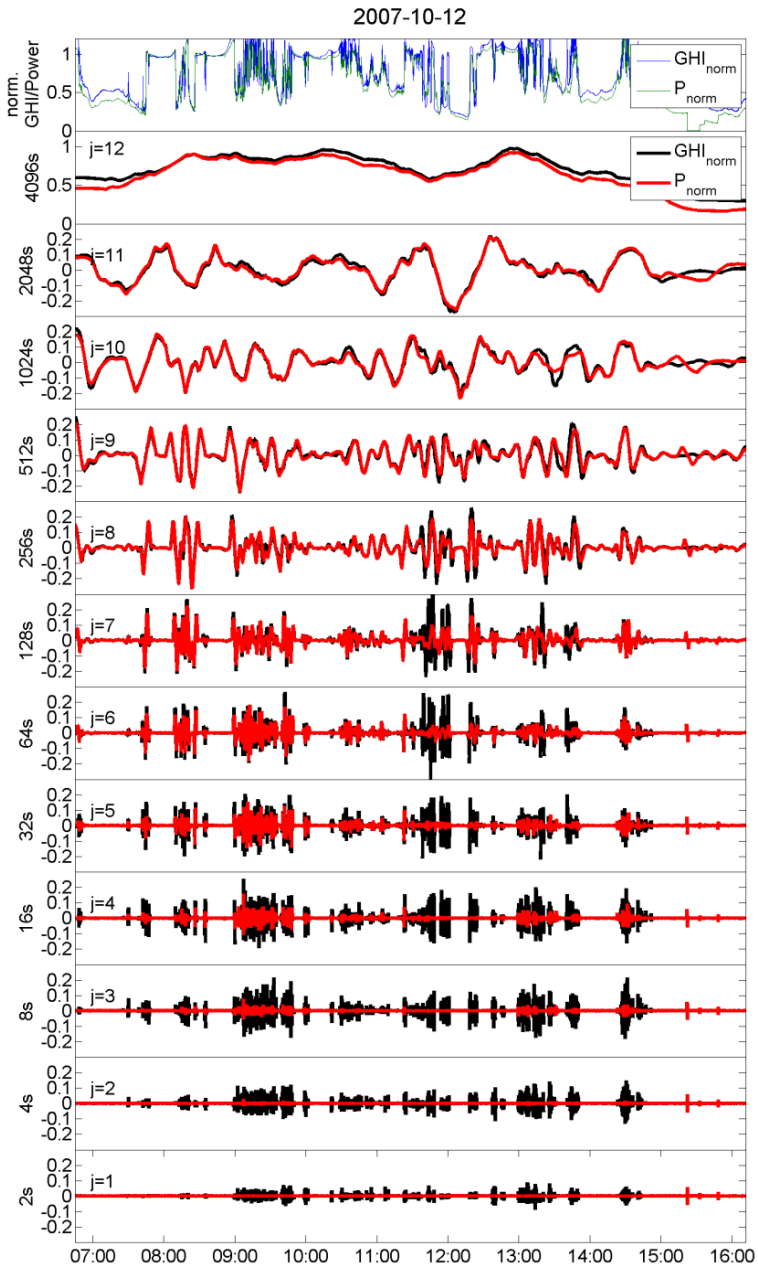

Figure 10. $\boldsymbol{GHI_{norm}}$ *and* $\boldsymbol{P_{norm}}$ *(top, blue and green lines), and their wavelet modes (black and red lines) on October 12, 2007. The* $\boldsymbol{j = 12}$ *mode is the moving average at 4096 sec, and it is included to illustrate that the sum of modes* $\boldsymbol{j = 1}$ *through* $\mathbf{12}$ *is equal to the original normalized signal.*

4.2.2 Fluctuation Power Content

One way to compare the wavelet modes of GHI_{norm} and P_{norm} is to calculate their mathematical fluctuation power content. Figure 11 shows the fluctuation power index (fpi) for GHI_{norm} and P_{norm}. Also included in Figure 11 are the fpis for the other five irradiance sensors at Pal Town, to ensure that the results are not biased by the use of only one of the six sensors. Although there are minor variations in the fpis of each of the six GHI sensors, the relationship between GHI fpi and Power fpi is very similar for all GHI sensors. At short timescales, the fluctuation power content is reduced significantly, up to a nearly 100 times reduction at the 2-sec timescale. At long timescales, fluctuation power indices, just as wavelet modes, are nearly identical.

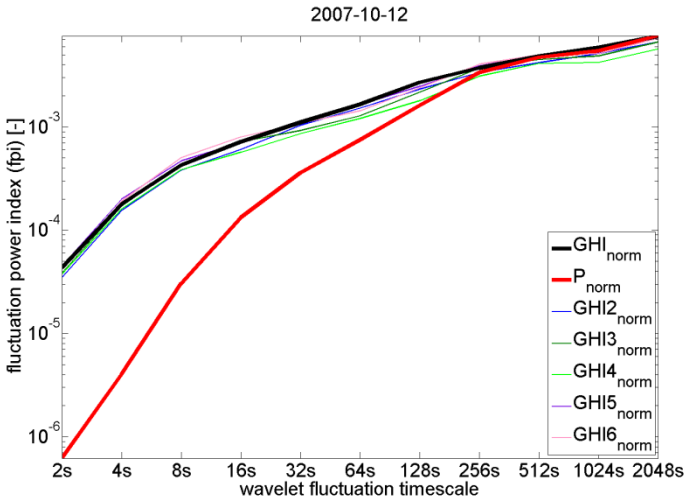

Figure 11. Wavelet fluctuation power index (fpi) of GHI_{norm} and P_{norm} (thick black and red lines) on October 12, 2007, on a logarithmic plot. Also included are the fpis from the five other irradiance sensors (thin colored lines).

4.2.3 Variability Reduction

For a numerical value on the benefit of geographic smoothing, the variability reduction (VR) between the first GHI point sensor and the total power output is computed. The VR as a function of timescale is shown in Figure 12. VR values of above 10 are found for timescales of 8 sec and shorter, confirming the extreme amounts of smoothing observed in Figures 10 and 11. At 256 sec (about 4 min), the VR is reduced to nearly 1. Therefore, it can be said that the longest timescales at which geographic smoothing is effective for Pal Town is about 128 sec (2 min). Beyond that timescale, the variability of the point sensor and the entire Pal Town system is comparable.

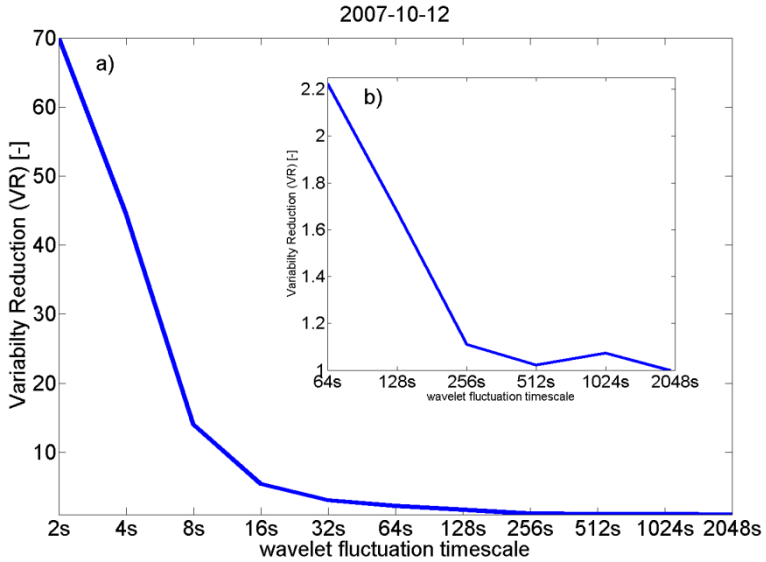

Figure 12. Variability reduction (VR) for $\boldsymbol{P_{norm}}$ versus $\boldsymbol{GHI_{norm}}$ for (a) all timescales and (b) zoomed in on timescales longer than 1 min. High values indicate the total power output was strongly smoothed over the GHI point sensor, while values of 1 indicate no smoothing.

5. CONCLUSION

The Pal Town neighborhood of Ota City, Japan, allowed for an in-depth study of a highly distributed 2-MW residential rooftop PV system. Although the data required a lot of quality control, the goals of characterizing the variability and determining how variability scales with the number of houses were achieved.

RR analysis focused on extreme ramps by studying the 99th-percentile RRs (RR99s). For a highly-variable test day, RR99s were found to initially decrease at all timescales as more houses were added, but a limit was reached where adding more houses had a very small effect on reducing RR99. The ratio of RR99 of one house to RR99 of many houses shows the effect of geographic smoothing on reducing ramp rates. Geographic smoothing was strong at 1 sec, reaching a 4.5 times reduction in RR99 of 477 houses versus a single house. At 10 min, however, the reduction on RR99 from adding more houses was very small, with RR99 reduced only about 10% for 477 houses over a single house. RR99s were plotted for all days with data in 2007, and similar trends were seen in other days, though the exact ratios of RR99s of one house versus many houses varied from day to day. The test day was found to have some of the highest RR99s of any day in 2007, confirming its use as a sample highly variable day. Based on the RR99s for all of 2007, the most extreme RRs over the whole year can be estimated.

By using a top hat wavelet transform, fluctuations over various timescales were resolved. While RRs include fluctuations of all timescales equal to and longer than the RR timescale, wavelet modes resolve only fluctuations at the timescale of interest. The fluctuations of the total power output of Pal Town were compared to the fluctuations of a single GHI point sensor, which represented a single house. At short timescales, fluctuations were up to 70 times reduced in the total power output over the GHI point sensor. The reduction in fluctuations, though, quickly decreased with increasing timescale. At times of 4 min and longer, there was very little difference in the wavelet fluctuations, and so the benefit of geographic smoothing was small at timescales longer than 4 min.

Overall, by studying this Ota City dataset, the following lessons were learned:

1. Extreme ramp rates tend to decrease with increasing levels of installed PV, due to geographic smoothing.
2. The incremental benefit of adding more houses with PV on reducing extreme ramp rates gets exponentially smaller as more houses are already in the system.
3. Short timescales show a larger reduction in extreme RRs when going from 1 to 500 houses than longer timescales.
4. Wavelet fluctuations, which show fluctuations isolated by timescale, are reduced at timescales shorter than 4 min, showing that clouds corresponding to timescales longer than 4 min are highly correlated at Pal Town.

6. REFERENCES

Curtright, A.E., and J. Apt, 2008. The character of power output from utility-scale photovoltaic systems. *Prog. Photovolt* 16, pp. 241-247.

Ineichen, P., and R. Perez, 2002. A new airmass independent formulation for the Linke turbidity coefficient. *Solar Energy* 73 (3), pp. 151-157.

Page, J., The role of solar radiation climatology in the design of photovoltaic systems, T. Markvart and L. Castaner, Editors, *Practical handbook of photovoltaics: fundamentals and applications*, Elsevier, Oxford (2003), pp. 5-66.

Lave, M., and J. Kleissl, 2010. Solar variability of four sites across the state of Colorado. *Renewable Energy* 35, pp. 2867-2873.

Lave, M., J. Kleissl, and E. Arias-Castro, 2011. High-frequency fluctuations and geographic smoothing. *Solar Energy* in press, doi:10.1016/j.solener.2011.06.031.

Mills, A., and R. Wiser, 2010. Implications of Wide-Area Geographic Diversity for Short-Term Variability of Solar Power. LBNL Report No. 3884E.

Murata, A., H. Yamaguchi, and K. Otani, 2009. A method of estimating the output fluctuation of many photovoltaic power generation systems dispersed in a wide area. *Electrical Engineering in Japan* 166 (4), pp. 9-19.

Otani, K., J. Minowa, and K. Kurokawa, 1997. Study of areal solar irradiance for analyzing areally-totalized PV systems. *Solar Energy Materials and Solar Cells* 47, pp. 281-288.

Perez, R., S. Kivalov, J. Schlemmer, C. Hemker, and T. Hoff, 2011. Short-term irradiance variability: Station pair correlation as a function of distance. Submitted to *Solar Energy*.

Wiemken, E., H.G. Beyer, W. Heydenreich, and K. Kiefer, 2001. Power characteristics of PV ensembles: experiences from the combined power production of 100 grid connected PV systems distributed over the area of Germany. *Solar Energy* 70 (6), pp. 513-518.

Woyte, A., R. Belmans, and J. Nijsb, 2007. Fluctuations in instantaneous clearness index: analysis and statistics. *Solar Energy* 81 (2), pp. 195-206.

DISTRIBUTION

External distribution *(distributed electronically unless otherwise noted)*:

3 U.S. Department of Energy
Solar Energy Technology Program
Attn: Kevin Lynn
Alvin Razon
Venkat Banunarayanan
950 L'Enfant Plaza
Washington, DC 20585

1 U.S. Department of Energy
Attn: Dan T. Ton
1000 Independence Ave. SW
EE-2A, FORS
Washington, DC 20585

1 U.S. Department of Energy/ALO
Attn: Dan Sanchez
Pennsylvania & H Street
Kirtland AFB, NZ-384-3
Albuquerque, NM 87184

1 UWIG
Attn: Charlie Smith
Utility Wind Integration Group
P.O. Box 2787
Reston, VA 20195

3 EPRI
Attn: Tom Key
Daniel Brooks
Jeff Smith
942 Corridor Park Blvd.
Knoxville, TN 37932

2 National Renewable Energy Laboratory
Attn: Brian Parson
Benjamin Kroposki
1617 Cole Blvd.
Golden, CO 80401-3305

1 Solar Electric Power Association
Attn: Julia Hamm, Executive Director
1220 19th St., Suite 401
Washington, DC 33708

1 University of California, San Diego
Attn: Jan Kleissl
9500 Gilman Dr.
La Jolla, CA 92093-0411

Internal distribution *(distributed electronically unless otherwise noted)*:

1	MS0321	Robert W. Leland	01400
1	MS0321	John L. Mitchiner	01460
1	MS0352	Jay Johnson	01718
1	MS0721	Marjorie L. Tatro	06100
1	MS0734	Ward I. Bower	06111
1	MS1033	Stanley Atcitty	06113
1	MS1033	Matthew Lave	06112
3	MS1033	Abraham Ellis	06112
1	MS1033	Jennifer E. Granata	06112
1	MS1033	Charles J. Hanley	06112
1	MS1033	Jimmy Quiroz	06112
1	MS1033	Joshua Stein	06112
1	MS1033	Cliff Hansen	06112
1	MS1082	Anthony L. Lentine	01727
1	MS1104	Rush D. Robinett III	06110
1	MS1108	Ross Guttromson	06113
1	MS1108	Juan J. Torres	06120
1	MS1318	Bruce A. Hendrickson	01440
1	MS1322	Sudip S. Dosanjh	01420
1	MS0899	RIM-Reports Management	9532 *(electronic copy)*


Sandia National Laboratories